Induction mapping of magnetostrictive materials

Jennifer Dooley
Jet Propulsion Laboratory, Pasadena, California 91109

Marc De Graef[a] and Michael E. McHenry
Department of Materials Science and Engineering, Carnegie Mellon, Pittsburgh, Pennsylvania 15213

An energy-filtered magnetic induction mapping technique has been implemented on a JEOL 4000EX equipped with a Gatan imaging filter. A study of the magnetic domain structure in Terfenol-D, a magnetostrictive actuator material, is presented as an example application of the technique. The method is equivalent to differential phase contrast microscopy by the reciprocity theorem. Image simulations of all stages of the induction mapping process are shown to support these observations. © *1998 American Institute of Physics.* [S0021-8979(98)47811-3]

INTRODUCTION

There is a growing interest in both room-temperature and very-low-temperature magnetostrictive actuator materials. Terfenol-D, a rare-earth transition-metal magnet, possesses a room-temperature magnetostrictive strain of about 0.2%, the largest known.[2] Ni_2MnGa exhibits large magnetostrictive strains, which arise from a magnetically induced martensitic transformation in a temperature range near room temperature.[3] Polycrystalline rare-earth low-temperature magnets have recently been shown to retain a significant fraction of the magnetostriction of the single crystals, and are considerably less expensive to produce.[4] Determination of the fine scale magnetic structure is essential for prediction of, among other things, the bulk magnetostrictive strains. In addition, since virtually all engineering parameters of these materials are directly affected by microstructural features, the nature of these materials makes it necessary to closely combine the study of magnetic structure and microstructure. Lorentz microscopy, in particular, the Fresnel and Foucault observation modes,[5] has for several decades been the dominant observation technique for qualitative magnetic domain observations.

The decreasing length scale of modern electronic and magnetic devices must be accompanied by improvements in the observation techniques used to study their micro- and nanostructures. The low-field sample environment and consequent increase in the focal length of the objective lens required for Lorentz microscopy results in a reduced final image magnification as compared to that of conventional transmission electron microscopy (TEM). This represents a serious limitation in the quantitative study of nanoscale magnetic structures. Furthermore, inelastic scattering in the sample contributes noise to the images, which further limits the attainable resolution of the standard Lorentz modes.

There are very few techniques capable of producing direct maps of the (in-plane) magnetic induction in a thin foil. Differential phase contrast (DPC) microscopy in a scanning TEM[7] is perhaps the most successful method, but it requires the installation of descanning coils and a four-quadrant detector, which are not accessible in the average research laboratory. For this method, the descanning coils are aligned such that any tilt of the beam arising from the scanning coils is compensated for at the plane of the quadrant detector so that any remaining shift of the beam over the detector is due to the Lorentz deflection. The magnitude of this deflection is measured as the difference signal from opposite quadrants of the detector and can be directly related to the components of the magnetic induction in two orthogonal directions $\pm U$ and $\pm V$. A technique equivalent to DPC by the reciprocity theorem for the TEM was proposed and implemented by Daykin and Petford-Long.[8] This induction mapping technique has been adapted to the 4000EX+GIF (Gatan imaging filter) combination, the method has been applied to the Terfenol-D system, and simulation algorithms have been created for the mapping technique.

EXPERIMENTAL METHODS

This article presents a summary of energy-filtered Lorentz observations of the Terfenol-D system. A Lorentz microscopy setup, which combines a high-resolution top-entry JEOL 4000EX TEM with a postcolumn GIF, has been previously reported.[6] With the main objective lens turned off, the sample is mounted in an essentially field-free region. The objective minilens, which sits below the plane of the specimen, provides sufficient field strength to focus the electrons into a diffraction pattern at the selected area aperture plane, thus providing Fresnel and Foucault observation modes. The energy filter provides an additional magnification of approximately 20×, and allows for the acquisition of zero-loss images, increasing the signal-to-noise ratio by at least an order of magnitude.[6] The magnetic resolution of this system is better than 5 nm.

All images in this paper were obtained from a thin foil of Terfenol-D, or $Tb_{0.73}Dy_{0.27}Fe_{1.95}$, which has a cubic Laves phase structure ($a = 0.732$ nm).[9] Single-crystal rods of Terfenol-D with [211] growth direction were obtained from Etrema, Inc. These were oriented by reflection Laue diffraction and cut into disks with [011] foil normal. Dimpled disks were then jet thinned in a chilled solution of 10% perchloric/90% acetic acid and ion milled for several hours with 4.5 kV

[a]Electronic mail: degraef@cmu.edu

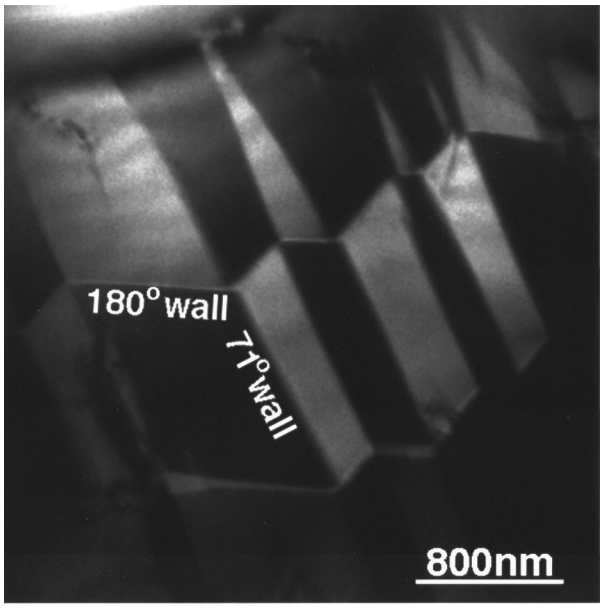

FIG. 1. Foucault image of a representative magnetic domain structure in Terfenol-D. This region is used in the induction maps of Fig. 2.

Ar^+ ions until electron transparent. For a detailed description of the microstructure of this material the reader is referred to Refs. 10, 11, and 6. Figure 1 shows a Foucault image of a characteristic lamellar domain arrangement. This area of the sample is used throughout the paper to illustrate the methods.

Magnetic induction mapping in the TEM was first introduced in Ref. 8 and adapted to the 4000EX+GIF combination in Ref. 6. A converged incident beam, with beam divergence angle θ_c, illuminates the region of interest on the sample. A small aperture truncates the transmitted beam in the back focal plane of the objective minilens and beam tilts are provided through the postspecimen image shift coils. The beam is tilted and images obtained with consecutive tilts are added together (approximating an integral with respect to beam tilt) and constitute the equivalent of the quadrant detector signals in DPC. For full details on the method the reader is referred to Ref. 12.

INDUCTION MAPPING RESULTS

Figure 2(a) shows four series of zero-loss Foucault images (slit width 15 eV), for two orthogonal tilt directions. The reader is referred to Ref. 12 for a description of the calibration of the tilt directions with respect to the microstructure. After aligning the Foucault images in each series they were summed on a per-pixel basis. The sums are shown in Fig. 2(b), along with the difference maps. Since the intensity in the difference map is proportional to the in-plane induction component in one of the two orthogonal directions, the difference maps can be represented as a single vector induction map, as shown in Fig. 2(c).

Using an image simulation algorithm developed by Mansuripur,[13] a method similar to standard high-resolution simulations has been implemented for the computation of magnetic induction tilt series and difference maps for a given magnetic structure.[12] The results are shown in Fig. 3. The

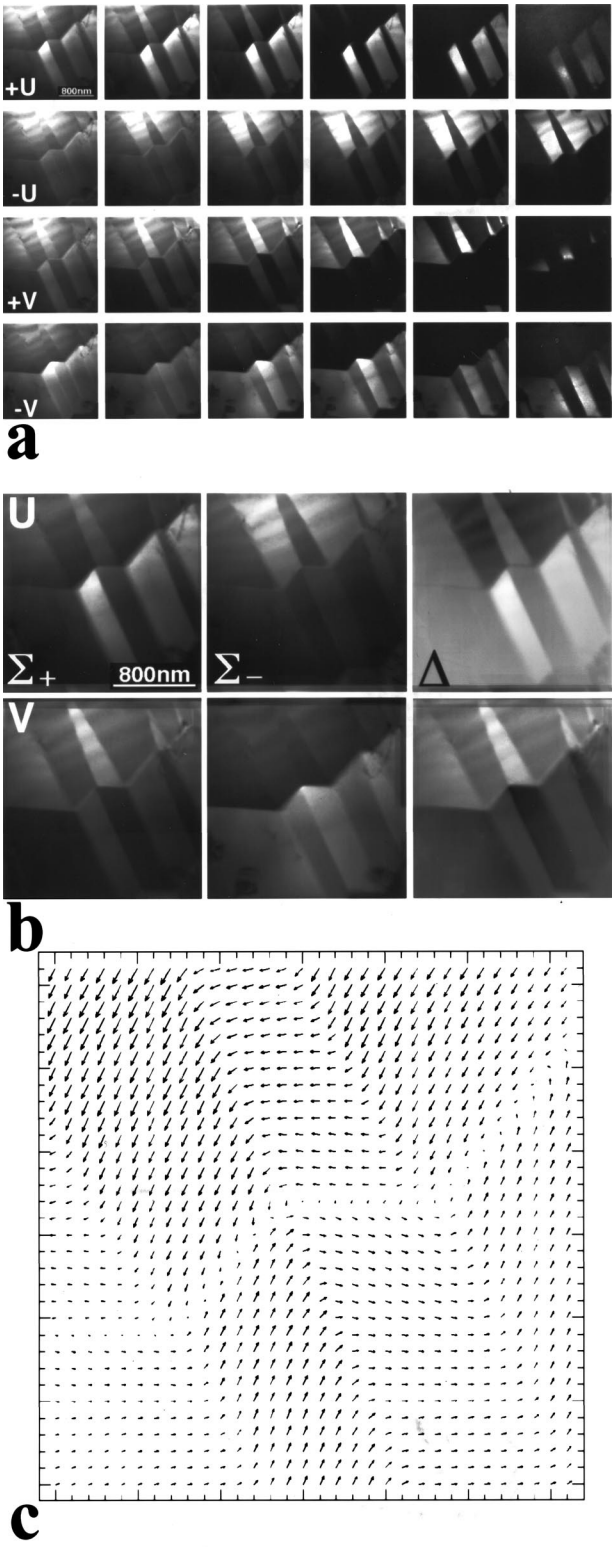

FIG. 2. (a) Foucault images as a function of postspecimen beam tilt for two orthogonal tilt directions. (b) Foucault sums and difference maps. (c) Vector induction map, created from the energy-filtered difference maps.

simulations were carried out for a 16 nm domain-wall width for the 180° Bloch-type wall, 10 nm for the 71° domain walls, a saturation magnetic induction of 1 T, foil thickness of 100 nm, beam divergence angle $\theta_c = 1$ mrad, a beam tilt increment of 3.5 μrad, aperture radius of 0.05 nm^{-1}, and an

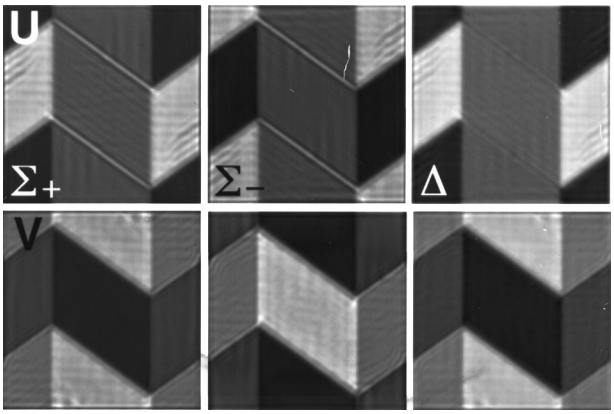

FIG. 3. Simulated summed tiltseries corresponding to Fig. 2(b); the top part of the simulated images is to be compared with the 180° domain-wall in Fig. 2(b).

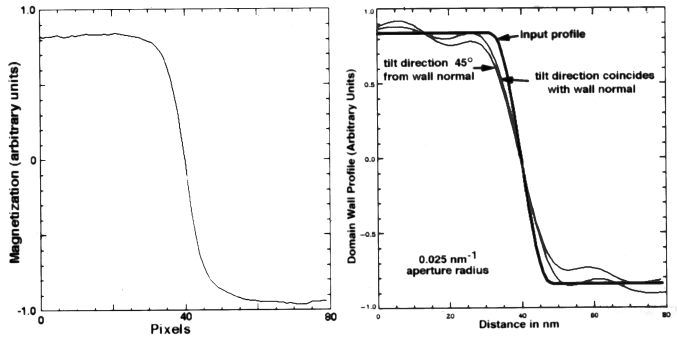

FIG. 4. (a) Line trace of the component of magnetic induction parallel to the domain wall averaged over 35 pixels and plotted over 80 pixels. (b) Comparison of the reconstructed magnetic induction component parallel to the 180° domain wall and the input profile.

incident beam energy of 400 kV. Tilt directions in the simulation were taken to be the same as in the experiment. The domain-wall profile from the filtered experimentally reconstructed map is shown in Fig. 4(a). The reconstructed 180° domain-wall width is estimated to be 83 nm, as each pixel corresponds to about 4.14 nm. For this case, one tilt direction was close to the normal of the domain wall. Figure 4(b) shows the simulated reconstructed map and the input profile.

Good qualitative agreement exists between these sets of images, including the presence of a faint bright fringe in the experimental $\pm U$ sums. The reconstructed vector map compares favorably with the experimental map in Fig. 2(b), as do the domain-wall profiles.

ACKNOWLEDGMENTS

The authors would like to thank N. T. Nuhfer for stimulating discussions, and N. Biery for providing the image alignment procedure used to compensate for image shifts during beam tilting. This work was supported in part by the National Science Foundation under Grant No. DMR 9403621 and by Rhône–Poulenc.

[1] G. F. Clark, B. K. Tanner, and H. T. Savage, Philos. Mag. B **46**, 331 (1982).
[2] D. C. Jiles, J. Phys. D **27**, 1 (1994).
[3] K. Ullakko, J. K. Huang, C. Kantner, R. C. O'Handley, and V. V. Kokorin, Appl. Phys. Lett. **69**, 1966 (1996).
[4] M. Q. Huang, Y. Zheng, and W. E. Wallace, J. Appl. Phys. **75**, 6280 (1994).
[5] L. Reimer, *Transmission Electron Microscopy* (Springer, Berlin, 1993).
[6] J. Dooley and M. De Graef, Ultramicroscopy **67**, 113 (1997).
[7] J. N. Chapman, P. E. Batson, E. M. Waddell, and R. P. Ferrier, Ultramicroscopy **3**, 203 (1978).
[8] A. Daykin and A. Petford-Long, Ultramicroscopy **58**, 365 (1995).
[9] M. Al-Jiboory and D. Lord, IEEE Trans. Magn. **26**, 2583 (1990).
[10] D. Lord, H. Savage, and R. Rosemeier, J. Magn. Magn. Mater. **29**, 137 (1982).
[11] R. James and D. Kinderlehrer, Philos. Mag. B **68**, 237 (1993).
[12] J. Dooley and M. De Graef, *Micron* (in press).
[13] M. Mansuripur, J. Appl. Phys. **69**, 2455 (1991).